A. Convergence of computational results

	average C_D	maximum C_L	St
Henderson (1995)	1.350	0.330[a]	0.166[a]
Tumkur *et al.* (2013)	1.360	0.328	0.168
Nek5000			
baseline[b]	1.381	0.340	0.167
larger domain[c]	1.364	0.338	0.166
finer mesh[d]	1.373	0.337	0.169
higher polynomial order[e]	1.372	0.336	0.169
smaller time step[f]	1.380	0.340	0.167

Table S1: Comparison of computed values of average drag coefficient (C_D), maximum lift coefficient (C_L), and Strouhal number (St) for flow past a fixed cylinder at $Re = 100$.

[a] Unpublished values quoted by Shiels, Leonard & Roshko (2001)
[b] domain: $24D \times 48D$; 3614 mesh elements; polynomial order 5; $\Delta\tau = 10^{-3}$
[c] baseline, except domain is $48D \times 63D$, and number of mesh elements increased to 8732 to preserve resolution
[d] baseline, except number of mesh elements increased to 8065
[e] baseline, except polynomial order increased to 7
[f] baseline, except time-step size reduced to $\Delta\tau = 5 \times 10^{-4}$

B. Recasting the eigenvalue problem

Beginning with the dimensionless governing equations (2.1a-d) and (2.4a,b), the lift coefficient C_L, and the boundary conditions

$$\mathbf{v}^*|_{cyl} = \frac{\mathrm{d}Y_1^*}{\mathrm{d}\tau}\mathbf{e}_y \tag{S1a}$$

and

$$\lim_{r\to\infty} \mathbf{v}^* = \mathbf{e}_x \tag{S1b}$$

in an inertial reference frame, we follow the approach of Tumkur *et al.* (2017) for the NES-less case, and transform the field equations of the full nonlinear problem to a coordinate system that moves with the cylinder according to

$$\mathbf{x}' = \mathbf{x} - Y_1(t)\mathbf{e}_y \tag{S2}$$

Dropping the asterisk on dimensionless quantities, and denoting by $'$ field quantities in the noninertial frame, we have

$$\frac{\partial \mathbf{v}'}{\partial \tau} + \frac{\mathrm{d}^2 Y_1}{\mathrm{d}\tau^2}\mathbf{e}_y + \mathbf{v}' \cdot \nabla \mathbf{v}' = -\nabla p' + \frac{1}{Re}\nabla^2 \mathbf{v}' \tag{S3a}$$

$$\frac{\mathrm{d}^2 Y_1}{\mathrm{d}\tau^2} + (2\pi f_n^*)^2 Y_1 = \frac{2C_L}{\pi m^*} + \epsilon_p \bar{r}_o \frac{\mathrm{d}}{\mathrm{d}\tau}\left(\frac{\mathrm{d}\theta}{\mathrm{d}\tau}\sin\theta\right) \tag{S3b}$$

$$\frac{\mathrm{d}^2\theta}{\mathrm{d}\tau^2} + \frac{\zeta_r}{Re}\frac{\mathrm{d}\theta}{\mathrm{d}\tau} = \frac{1}{\bar{r}_o}\frac{\mathrm{d}^2 Y_1}{\mathrm{d}\tau^2}\sin\theta \tag{S3c}$$

where

$$C_L = \frac{2}{Re}\int_0^{2\pi}\left[-\left.\frac{\partial\omega^{'}}{\partial r}\right|_{cyl} + \omega^{'}_{cyl}\right]\cos\phi\ \mathrm{d}\phi \tag{S4}$$

subject to the boundary conditions

$$\mathbf{v}^*|_{cyl} = \mathbf{0} \tag{S5}$$

and

$$\lim_{r\to\infty}\mathbf{v}^{'} = \mathbf{e}_x + \frac{\mathrm{d}Y_1}{\mathrm{d}\tau}\mathbf{e}_y \tag{S6}$$

The cylinder displacement and NES position are not field variables, and are unaffected by the transformation (S4). Note also that the vorticity is the curl of the velocity field, and is thus invariant under this transformation.

Now, consider the linear stability problem, and write

$$\begin{bmatrix}\mathbf{v}^{'}(r,\phi,\tau)\\ p^{'}(r,\phi,\tau)\\ Y_1(\tau)\\ \theta(\tau)\end{bmatrix} = \begin{bmatrix}\mathbf{v}_s(r,\phi)\\ p_s(r,\phi)\\ 0\\ \theta_s\end{bmatrix} + \begin{bmatrix}\hat{\mathbf{v}}(r,\phi)\\ \hat{p}(r,\phi)\\ \hat{Y}\\ \hat{\theta}\end{bmatrix} e^{\sigma\tau} \tag{S7}$$

where the subscript s denotes a value corresponding to a steady solution of the full nonlinear equations, and the hatted quantities denote infinitesimal disturbances. Linearizing about the steady solution, we have

$$\sigma\hat{\mathbf{v}} + \hat{\mathbf{v}}\cdot\nabla\mathbf{v}_s + \mathbf{v}_s\cdot\nabla\hat{\mathbf{v}} + \sigma^2\hat{Y}\mathbf{e}_y = -\nabla\hat{p} + \frac{1}{Re}\nabla^2\hat{\mathbf{v}} \tag{S8a}$$

$$\sigma^2\hat{Y} + (2\pi f_n^*)^2\hat{Y} = \frac{4\int_0^{2\pi}\left[-\left.\frac{\partial\hat{\omega}}{\partial r}\right|_{cyl} + \hat{\omega}_{cyl}\right]\cos\phi\ \mathrm{d}\phi}{\pi m^* Re} + \epsilon_p\bar{r}_o\sigma^2\hat{\theta}\sin\theta_s \tag{S8b}$$

$$\sigma^2\hat{\theta} + \sigma\frac{\zeta_r}{Re}\hat{\theta} = \frac{1}{\bar{r}_o}\sigma^2\hat{Y}\sin\theta_s \tag{S8c}$$

subject to the boundary conditions

$$\mathbf{v}^*|_{cyl} = \mathbf{0} \tag{S9}$$

$$\lim_{r\to\infty}\hat{\mathbf{v}} = \sigma\hat{Y}\mathbf{e}_y \tag{S10}$$

Solving for $\hat{\theta}$, we get

$$\hat{\theta} = \frac{\sigma^2\hat{Y}\sin\theta_s}{\bar{r}_o\left(\sigma^2 + \sigma\zeta_r/Re\right)} = \frac{\sigma\hat{Y}\sin\theta_s}{\bar{r}_o\left(\sigma + \zeta_r/Re\right)} \tag{S11}$$

so that

$$\sigma^2\hat{Y} + (2\pi f_n^*)^2\hat{Y} = \frac{4\int_0^{2\pi}\left[-\frac{\partial\hat{\omega}}{\partial r}\big|_{cyl} + \hat{\omega}_{cyl}\right]\cos\phi\ \mathrm{d}\phi}{\pi m^* Re} + \epsilon_p\bar{r}_o\frac{\sigma^3\hat{Y}\sin^2\theta_s}{\bar{r}_o\left(\sigma + \zeta_r/Re\right)} \tag{S12}$$

We solve (S12) for $\hat{Y}$ and get

$$\hat{Y} = \frac{4\int_0^{2\pi}\left[-\frac{\partial\hat{\omega}}{\partial r}\big|_{cyl} + \hat{\omega}_{cyl}\right]\cos\phi\ \mathrm{d}\phi}{\pi m^* Re\left[\sigma^2 + (2\pi f_n^*)^2 - \epsilon_p\frac{\sigma^3\sin^2\theta_s}{\sigma+\zeta_r/Re}\right]} \tag{S13}$$

Hence, we have

$$\sigma\hat{\mathbf{v}} + \hat{\mathbf{v}}\cdot\nabla\mathbf{v}_s + \mathbf{v}_s\cdot\nabla\hat{\mathbf{v}} + \frac{4\sigma^2\int_0^{2\pi}\left[-\frac{\partial\hat{\omega}}{\partial r}\big|_{cyl} + \hat{\omega}_{cyl}\right]\cos\phi\ \mathrm{d}\phi}{\pi m^* Re\left[\sigma^2 + (2\pi f_n^*)^2 - \epsilon_p\frac{\sigma^3\sin^2\theta_s}{\sigma+\zeta_r/Re}\right]}\mathbf{e}_y = -\nabla\hat{p} + \frac{1}{Re}\nabla^2\hat{\mathbf{v}} \tag{S14}$$

subject to the boundary conditions

$$\hat{\mathbf{v}}(1/2,\phi) = \mathbf{0} \tag{S15}$$

$$\lim_{r\to\infty}\hat{\mathbf{v}} = \frac{4\sigma^2\int_0^{2\pi}\left[-\frac{\partial\hat{\omega}}{\partial r}\big|_{cyl} + \hat{\omega}_{cyl}\right]\cos\phi\ \mathrm{d}\phi}{\pi m^* Re\left[\sigma^2 + (2\pi f_n^*)^2 - \epsilon_p\frac{\sigma^3\sin^2\theta_s}{\sigma+\zeta_r/Re}\right]}\mathbf{e}_y \tag{S16}$$

We now make the following observations. First, Eqs. (S14) and (S16) show that the linear stability of the steady solution is independent of the radius ratio $\bar{r}_o$. Second, although linear stability depends on the value of the NES displacement, θ_s, that dependence can be absorbed into a dependence on $\epsilon_p\sin^2\theta_s$, so that there are are only two additional independent parameters upon which stability depends, namely ζ_r and $\epsilon_p\sin^2\theta_s$. We also note that for $\theta_s = 0$ or π, or for $\epsilon_p = 0$, the NES has no effect on the linear stability problem, which reduces to the NES-less case for a sprung cylinder. Third, Eqs. (S14) and (S16) show that the critical Re for the NES case will asymptotically approach that of the NES-less sprung-cylinder case either as the damping coefficient $\zeta_r \to \infty$ or $\epsilon_p\sin^2\theta_s \to 0$.

C. Results for initial NES mass displacement of $\pi/4$

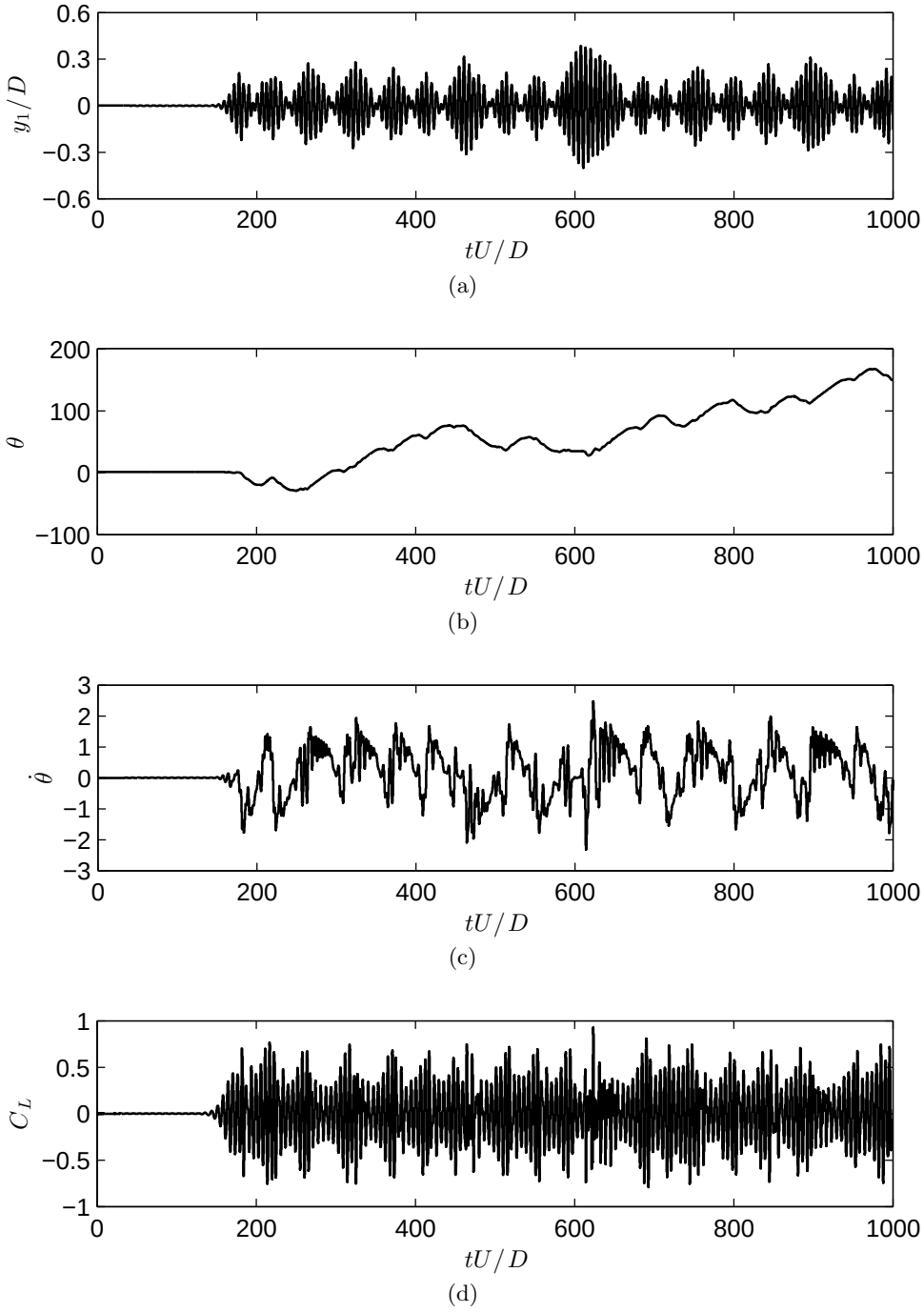

Figure S1: Mechanism I with $\theta(t = 0) = \pi/4$ for $Re = 100$, $\bar{r}_o = 0.2$, $\epsilon_p = 0.3$, and $\zeta_r = 21.221$. (a) cylinder displacement (Y_1); (b) NES angle (θ); (c) NES angular velocity ($\dot{\theta}$); and (d) lift coefficient (C_L). Root-mean-square values of Y_1 and C_L for $200 \leqslant tU/D \leqslant 1000$ are 0.1182 and 0.3328, respectively.

D. Response of an NES-less cylinder at $Re = 60$

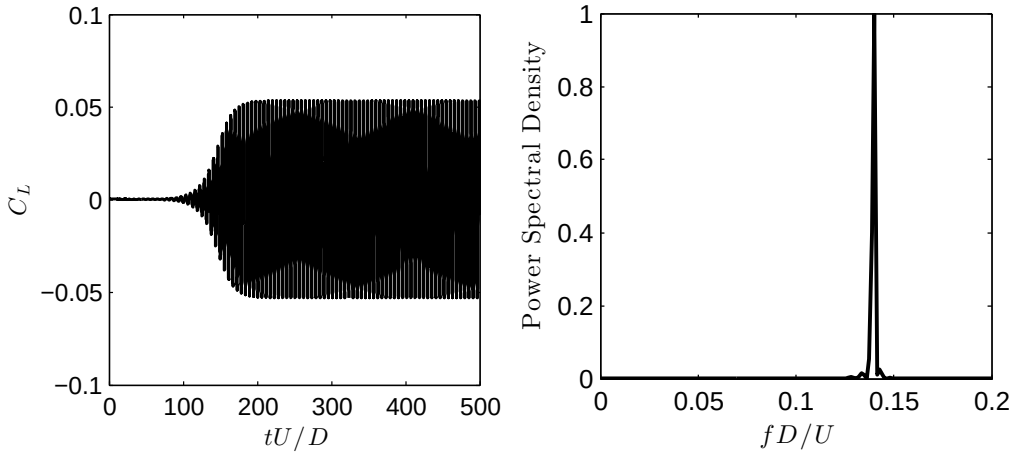

(a) (b)

Figure S2: For a stationary cylinder at $Re = 60$, (a) lift coefficient (C_L) and (b) frequency of lift coefficient (Strouhal number).

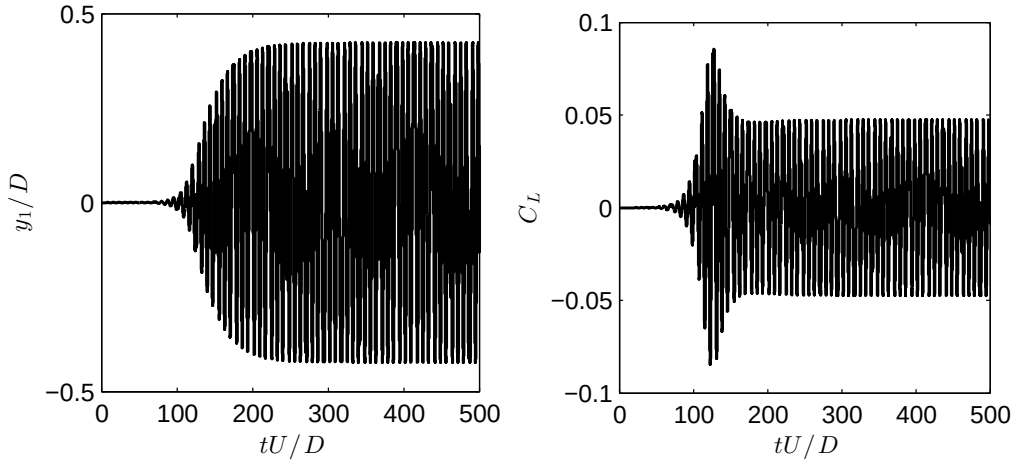

(a) (b)

Figure S3: VIV at $Re = 60$ and $f_n^* = 0.14$ with no NES. (a) cylinder displacement (Y_1) and (b) lift coefficient (C_L).

E. Convergence of correlation dimension

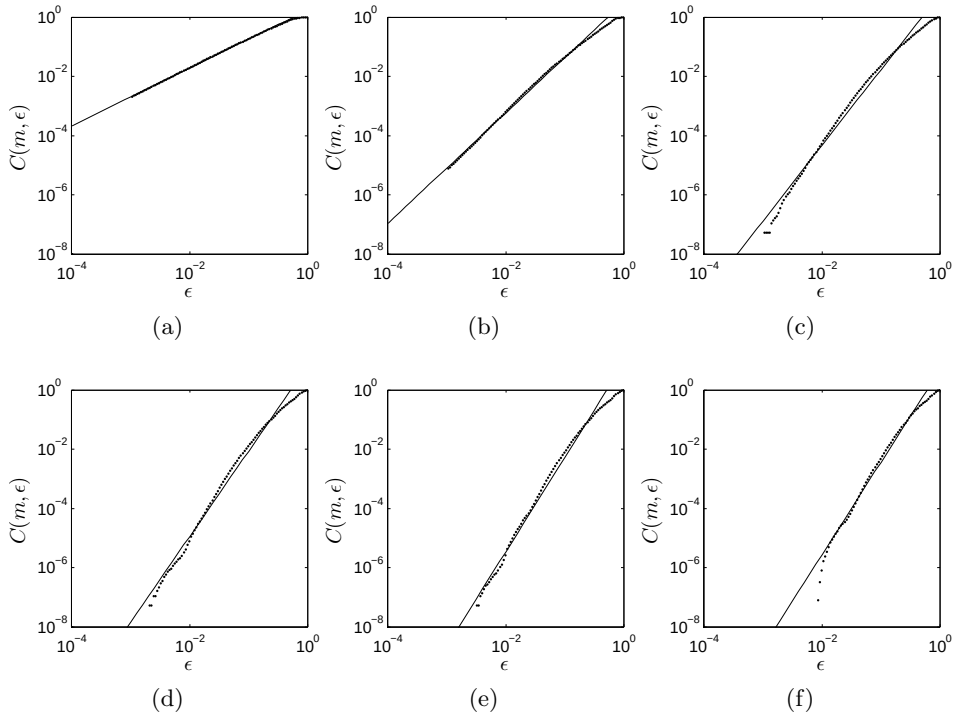

Figure S4: For $Re = 100$, $\bar{r}_o = 0.5$, $\epsilon_p = 0.3$, and $\zeta_r = 0.340$, convergence of correlation dimension D_{corr} (slope of least-squares fitted line to correlation sum data) with increase in embedding dimension m: $\cdots$, $C_m(\sigma)$; —, least-squares fit for $C_m(\sigma)$ computed for the range of σ shown. (a) $m = 1$, $D_{corr} = 0.9743$. (b) $m = 2$, $D_{corr} = 1.8626$. (c) $m = 3$, $D_{corr} = 2.5524$. (d) $m = 4$, $D_{corr} = 2.8813$. (e) $m = 5$, $D_{corr} = 3.1818$. (f) $m = 6$, $D_{corr} = 3.1219$.

F. Experimental realization

In order to establish the relationship between a rotating NES with a distributed rotating mass and one with rotating mass concentrated on a line or at a point, Steytler & Pearlstein (2016) have extended the analysis of Gendelman *et al.* (2012) for a point mass m rotating at fixed radius about a fixed axis perpendicular to the rectilinear motion of a (nonrotating) "primary" mass M, and established relationships between the inertial properties of the rotating distributed mass and the mass of the "primary structure" (referred to in the main text as the "stator)," which guarantee dynamic equivalence (defined in §6.3 of the main text) between the concentrated- and distributed-mass cases.

For the point-mass case, the dimensionless dynamical equations developed by Gendelman *et al.* (2012) [their equation (5)] for the free response are

$$\frac{\mathrm{d}^2 u}{\mathrm{d}t^2} + u = \epsilon_p \frac{\mathrm{d}}{\mathrm{d}t}\left(\frac{\mathrm{d}\theta}{\mathrm{d}t}\sin\theta\right) \tag{S17a}$$

$$\frac{\mathrm{d}^2\theta}{\mathrm{d}t^2} + \lambda\frac{\mathrm{d}\theta}{\mathrm{d}t} = \epsilon_p\frac{\mathrm{d}^2u}{\mathrm{d}t^2}\sin\theta \tag{S17b}$$

in which $\epsilon_p = m_p/(m_p + M)$ is the fraction of the total mass comprised by the rotating point mass, and the rectilinear displacement and time have been nondimensionalized using the radial location of the point mass r_o, and $\sqrt{(m+M)/K}$, respectively. In contrast, for the distributed-mass case, dimensionless equations for the free response are

$$\frac{\mathrm{d}^2\xi}{\mathrm{d}\tau^2} + \xi = \frac{R_{cm}^2}{R_g^2}\epsilon_d\frac{\mathrm{d}}{\mathrm{d}\tau}\left(\frac{\mathrm{d}\theta}{\mathrm{d}\tau}\sin\theta\right) \tag{S18a}$$

$$\frac{\mathrm{d}^2\theta}{\mathrm{d}\tau^2} + \hat{\lambda}\frac{\mathrm{d}\theta}{\mathrm{d}\tau} = \frac{\mathrm{d}^2\xi}{\mathrm{d}\tau^2}\sin\theta \tag{S18b}$$

Here, R_{cm} is the distance from the axis of rotation to the center of mass, R_g is the radius of gyration, $\epsilon_d = m_d/\left(M + m_d\right)$, m_d is the mass of the rotating distributed mass, and $\hat{\lambda}$ is a dimensionless damping coefficient. In the distributed-mass case, the relationship between the free-response equations (S18a,b) and the ODEs for the cylinder and rotating-mass dynamics under VIV loading is precisely analogous to the corresponding relationship for the point-mass case [i.e., (S17a,b) and (2.4a,b)], so that we have

$$\frac{\mathrm{d}^2Y_1}{\mathrm{d}\tau^2} + \left(2\pi f_n^*\right)^2 Y_1 = \frac{2C_L}{\pi m^*} + \frac{R_{cm}}{D}\epsilon_d\frac{\mathrm{d}}{\mathrm{d}\tau}\left(\frac{\mathrm{d}\theta}{\mathrm{d}\tau}\sin\theta\right) \tag{S19a}$$

$$\frac{\mathrm{d}^2\theta}{\mathrm{d}\tau^2} + \frac{\zeta_r}{Re}\frac{\mathrm{d}\theta}{\mathrm{d}\tau} = \frac{D}{R_{cm}}\frac{R_{cm}^2}{R_g^2}\frac{\mathrm{d}^2Y_1}{\mathrm{d}\tau^2}\sin\theta \tag{S19b}$$

where the rectilinear displacement and time are nondimensionalized by the cylinder diameter D, and D/U, respectively. (Note that if the rectilinear displacement had been nondimensionalized using R_g, R_{cm}, or any length scale involving either R_g or R_{cm}, the boundary condition 2.1c would involve R_g or R_{cm}, and would thus depend on the inertial properties of the rotating mass.)

Comparison of distributed-mass equations S19a and S19b to the point-mass equations 2.4a and 2.4b shows that the two will be dynamically equivalent if

$$\epsilon_p\bar{r}_o = \epsilon_d R_{cm}/D \tag{S20a}$$

and

$$\bar{r}_o = (R_{cm}/D)(R_g^2/R_{cm}^2) \tag{S20b}$$

We observe that $\epsilon_p = \epsilon_d$ is possible only if $R_g = R_{cm}$. But the parallel axis theorem (Kleppner & Kolenkow 1973) shows that this is possible only for a point mass. Thus, for a distributed-mass rotating NES, the required mass ratio $m/\left(m + M\right)$ will necessarily differ from the point-mass value if dynamic equivalence is to be achieved.

Since most of the results in the paper are for $Re = 100$, we consider that Re. To keep the NES (and its rotating mass) inside the cylinder, we choose a fairly large cylinder diameter, 10 cm, which avoids small clearances, and simplifies construction.

This size is also convenient for visualization and optical diagnostics in a number of water-tunnel facilities. For $Re = 100$ and $D = 10$ cm, the experimentally convenient free-stream velocity of 35 cm/s corresponds to a kinematic viscosity of 350 cSt, well within the range of a variety of commercially available mineral oils, lubricating oils, silicone oils, and heat transfer fluids. We consider SAE 30, for which the viscosity and density at 20° C are 350 cSt and 0.89 g cm^{-3}, respectively. Our density ratio of 10 corresponds to a cylinder density of 8.9 g cm^{-3}. Taking the rotating mass to be a cylinder of density ρ_{rnes} whose cross section is an annular sector with inner and outer radii R_1 and R_2, respectively, and sector angle α, and the stator to be a cylindrical annulus with inner and outer radii R_{stat} and $R = D/2$, respectively, and density ρ_{rnes}, it follows that

$$8.9 \text{ g cm}^{-3} \left(\pi R^2\right) = \rho_{rnes} \left(R_2^2 - R_1^2\right) \frac{\alpha}{2} + \rho_{stat} \pi \left(R^2 - R_{stat}^2\right) \tag{S21}$$

Nondimensionalizing (S21), we find

$$8.9 = \chi_{rnes} \left(\eta_2^2 - \eta_1^2\right) \frac{\alpha}{2\pi} + \chi_{rnes} \left(1 - \eta_{stat}^2\right) \tag{S22}$$

where we define $\eta_1 = R_1/R, \eta_2 = R_2/R, \eta_{stat} = R_{stat}/R, \chi_{rnes} = \rho_{rnes}$ cm^3 g^{-1} and $\chi_{stat} = \rho_{stat}$ cm^3 g^{-1}. The radial location of the center of mass of the annular sector, R_{cm}, is found by completing the centroid, while the radius of gyration is found from $R_g = \sqrt{\hat{I}_{zz}/\hat{M}_{rnes}}$, where $\hat{I}_{zz}$ is the moment of inertia per unit length, taken about the cylinder axis. Performing those two straightforward integrations, we have

$$\frac{R_{cm}}{D} = \frac{2 \sin\left(\alpha/2\right) \left(\eta_1^2 + \eta_1 \eta_2 + \eta_2^2\right)}{3\alpha \left(\eta_1 + \eta_2\right)} \tag{S23a}$$

and

$$\frac{R_{cm}}{R_g} = \frac{4\sqrt{2} \sin\left(\alpha/2\right) \left(\eta_1^2 + \eta_1 \eta_2 + \eta_2^2\right)}{\alpha \left(\eta_1 + \eta_2\right) \sqrt{\eta_1^2 + \eta_2^2}} \tag{S23b}$$

For given values of the parameters ϵ_p and $\bar{r}_o$ in the point-mass approximation, the objective is to find values of $\eta_1 \leqslant \eta_2 \leqslant \eta_{stat}$, α, χ_{rnes}, and χ_{stat} such that (S20a, S20b, and S22) are satisfied, where

$$\begin{aligned} \epsilon_d &= \frac{\rho_{rnes}(R_2^2 - R_1^2)\frac{\alpha}{2}}{\rho_{rnes}(R_2^2 - R_1^2)\frac{\alpha}{2} + \pi\rho_{stat}\left(R^2 - R_{stat}^2\right)} \\ &= \frac{\chi_{rnes}\left(\eta_2^2 - \eta_1^2\right)\frac{\alpha}{2\pi}}{\chi_{rnes}\left(\eta_2^2 - \eta_1^2\right)\frac{\alpha}{2\pi} + \chi_{stat}\left(1 - \eta_{stat}^2\right)} \end{aligned} \tag{S24}$$

We consider (S20a, S20b, and S22) to be three equations in six unknowns, from which it follows that there is a three-parameter family of solutions.

In seeking solutions, it is important to keep in mind that the densest material that can practicably be used is tungsten, with a density of 19.3 g cm^{-3}, (Tungsten is routinely used as a ballast in aircraft and other applications. Other elements and their alloys have densities as high as 22.6 g cm^{-3}, but are much more expensive.)

For the values of ϵ_p and $\bar{r}_o$ (0.3 and 0.47, respectively) used to compute the chaotic results in figure 16, a solution is $\eta_1 = 0.2$, $\eta_2 = 0.855568$, $\eta_{stat} = 0.9143295$,

$\alpha = 2.8754087$ radians, $\chi_{rnes} = 19.3000$, and $\chi_{stat} = 17.0000$. The values of the geometric parameters η_1, η_2, η_{stat}, and α were chosen to satisfy (S20a, S20b, and S22), subject to (S23a, S23b, S24), and to give densities very close to those of elemental tungsten and two commercially available tungsten alloys (0.9 W, 0.06 Ni, 0.04 Cu; and 0.9 W, 0.07 Ni, 0.03 Fe), both having a density of 17.0 g cm^{-3}. For a cylinder with a 10 cm diameter, this gives inner and outer radii of 1.0 cm and 4.27784 cm, respectively, and a sector angle of 2.8754087 radians for the rotating mass, and inner and outer radii of 4.571647 cm and 5 cm, respectively for the stator, with a clearance of $(\eta_{stat} - \eta_2)\,(10\text{ cm}/2) = 2.94$ mm between the rotating mass and the stator that should be adequate. For this distributed-mass choice, the ratio of the rotating mass to the overall mass is $\epsilon_d = 0.686739$, more than twice the value for the dynamically equivalent point-mass model ($\epsilon_p = 0.3$).

REFERENCES

Anagnostopoulos, P. 2000*a* Numerical study of the flow past a cylinder excited transversely to the incident stream. Part 1: Lock-in zone, hydrodynamic forces and wake geometry. *J. Fluids Struct.* **14**, 819–851.

Anagnostopoulos, P. 2000*b* Numerical study of the flow past a cylinder excited transversely to the incident stream. Part 2: Timing of vortex shedding, aperiodic phenomena and wake parameters. *J. Fluids Struct.* **14**, 853–882.

Cossu, C. & Morino, L. 2000 On the instability of a spring-mounted circular cylinder in a viscous flow at low reynolds numbers. *Journal of Fluids and Structures* **14**, 183–196.

Gendelman, O. V., Sigalov, G., Manevitch, L. I., Mane, M., Vakakis, A. F. & Bergman, L. A. 2012 Dynamics of an eccentric rotational nonlinear energy sink. *Journal of Applied Mechanics* **79**, 011012–9.

Henderson, R. D. 1995 Details of the drag curve near the onset of vortex shedding. *Phys. of Fluids* **7**, 2102–2104.

Kleppner, D. & Kolenkow 1973 *An Introduction to Mechanics*. McGraw-Hill.

Li, Jing, Sun, Jiong & Roux, Bernard 1992 Numerical study of an oscillating cylinder in uniform flow and in the wake of an upstream cylinder. *JFM* **237**, 457–478.

Nakano, M. & Rockwell, D. 1994 Flow structure in the frequency-modulated wake of a cylinder. *JFM* **266**, 93–119.

Olinger, D. J. & Sreenivasan, K. R. 1988 Nonlinear dynamics of the wake of an oscillating cylinder. *Phys. Rev. Lett.* **60**, 797–800.

Shiels, D., Leonard, A. & Roshko, A. 2001 Flow-induced vibration of a circular cylinder at limiting structural parameters. *J. Fluids Struct.* **15**, 3–21.

Steytler, L. L. & Pearlstein, A. J. 2016 *Distributed-mass rotating nonlinear energy sinks*. In preparation.

Tumkur, R. K. R., Calderer, R., Masud, A., Pearlstein, A. J., Bergman, L. A. & Vakakis, A. F. 2013 Computational study of vortex-induced vibration of a sprung rigid circular cylinder with a strongly nonlinear internal attachment. *J. Fluids Struct.* **40**, 214–232.

Tumkur, R. K. R., Fischer, P. F., Bergman, L. A., Vakakis, A. F. & Pearlstein, A. J. 2017 Stability of the steady, two-dimensional flow past a linearly-sprung circular cylinder. *J. Fluid Mech.* Submitted.